Geomech. Geophys. Geo-energ. Geo-resour. (2020) 6:28
https://doi.org/10.1007/s40948-020-00153-1

ORIGINAL ARTICLE

Effect of slick-water fracturing fluid on the frictional properties of shale reservoir rock gouges

Mengke An · Haoyong Huang · Fengshou Zhang · Derek Elsworth

Received: 2 January 2020 / Accepted: 26 February 2020

Abstract "Slick-water" fluids routinely used in hydraulic fracturing contain friction-reducing agents and clay-stabilizers that may influence on the strength and stability of reservoir rocks and preexisting faults. We performed laboratory measurements on four powered shale reservoir rocks with different carbonate contents recovered from Longmaxi Formation in Sichuan Basin of China, to examine the potential effects of slick-water fracturing fluids on gouge friction. Velocity-stepping experiments were conducted at shear velocities of 0.122 and 1.22 μm/s, a confining pressure of 60 MPa, a pore fluid pressure of 30 MPa and a temperature of 90 °C, typifying the ~ 2.3 km depth of producing reservoirs. Two pore fluids, i.e., DI water and acidic slick-water, were selected to probe the chemical effects of fracturing fluids. Results show that the frictional properties of studied shale gouges are not only controlled by both the phyllosilicate and carbonate contents, but also affected by slick-water. Acidic slick-water dissolves carbonates from the shale gouges and this mineralogic alteration exerts a negligible influence on frictional strength μ but increases the frictional stability $(a - b)$, regardless of the mass of carbonate removed. Clay stabilizers are shown to exert minimal influence on either frictional strength or stability at high confined stresses, possibly due to the unchanged mineral contacts. Our results imply that the acidity of slick-water fluids can impact the frictional responses in carbonate-rich fault gouges through corrosion and dissolution, and have important implications in understanding the chemical effects from the fracturing fluids on subsurface fault stability during shale reservoir stimulation.

Keywords Slick-water · Fracturing · Shale · Fault gouge · Strength and stability · Clay swelling

M. An · F. Zhang (✉)
Department of Geotechnical Engineering, College of Civil Engineering, Tongji University, Shanghai 200092, China
e-mail: fengshou.zhang@tongji.edu.cn

M. An · F. Zhang
Key Laboratory of Geotechnical and Underground Engineering of Ministry of Education, Tongji University, Shanghai 200092, China

H. Huang
Shale Gas Research Institute, PetroChina Southwest Oil and Gasfield Company, Chengdu 610051, China

D. Elsworth
Department of Energy and Mineral Engineering, EMS Energy Institute and G3 Center, The Pennsylvania State University, University Park, PA 16802, USA

D. Elsworth
Department of Geosciences, The Pennsylvania State University, University Park, PA 16802, USA

Published online: 03 March 2020

1 Introduction

The recovery of natural gas from shale reservoirs has been facilitated by the advent of horizontal drilling combined with massive hydraulic fracturing (Clark 1949; Grossman 1951). During hydraulic fracturing, high-pressure fracturing fluid is injected into a targeted zone of the reservoir to drive the propagation of an hydraulic fracture and thereby enhance reservoir permeability (Rubinstein and Mahani 2015; Zhang et al. 2017a). Generally, 4 to 6 million gallons are injected during shale reservoir stimulation (Al-Muntasheri 2014). However, a significant proportion of the fracturing fluid (up to 90%) may be retained within the reservoir with only a small proportion returning in the flow-back water (Vidic et al. 2013). "Slick-water" is one frequently used fracturing fluid where friction-reducing agents are used to reduce frictional losses along the wellbore and thereby allow the full injection pressure to be applied at the heel of the hydraulic fracture, along the wellbore (Yang et al. 2013). The remnant slick-water fracturing fluid that remains and penetrates the reservoir may exert significant physical and chemical controls on the frictional strength and stability of the shale reservoir rocks (Arthur et al. 2011; Jacoby 2011).

During the hydraulic fracturing phase, the injection well may be close to, or directly transect, a preexisting natural fault at depth (Fig. 1a). The slick-water fracturing fluid may penetrate the adjacent fault gouge zone through the conduit itself, or through natural or hydraulic fractures (Fig. 1b) (Davies et al. 2013; Scuderi and Collettini 2018; Guindon 2015) (Fig. 1b). The slick-water in the fault gouge zone could have several adverse impacts on the stability of gouge-filled faults. First, the slick-water could lubricate the fault and reduce the fault frictional strength (Diao and Espinosa-Marzal 2018). Second, the slick-water infiltrating the fault zone may elevate local pore fluid pressures. This fluid overpressure can promote fault reactivation (Scuderi et al. 2017). Third, typical shales span a wide range of mineralogical compositions (Kohli and Zoback 2013), enabling acidic friction-reducers and clay-stabilizers to potentially react with the fault gouge and alter the mineral composition (Dieterich et al. 2016; Pedlow and Sharma 2014) and frictional strength and stability (Fang et al. 2018; Zhang et al. 2019).

Significant efforts have been applied to understand the interaction between slick-water fracturing fluids and the physical properties of shales. These include the impacts of the removal of carbonate minerals in altering pore structure (Sun et al. 2018; Wu and Sharma 2017), with concomitant impact on gas transport and hydrocarbon permeability (Pagels et al. 2013). Halide clay stabilizers minimize clay swelling and significantly enhance the tensile strength of shale samples (Aderibigbe and Lane 2013; Huang et al.

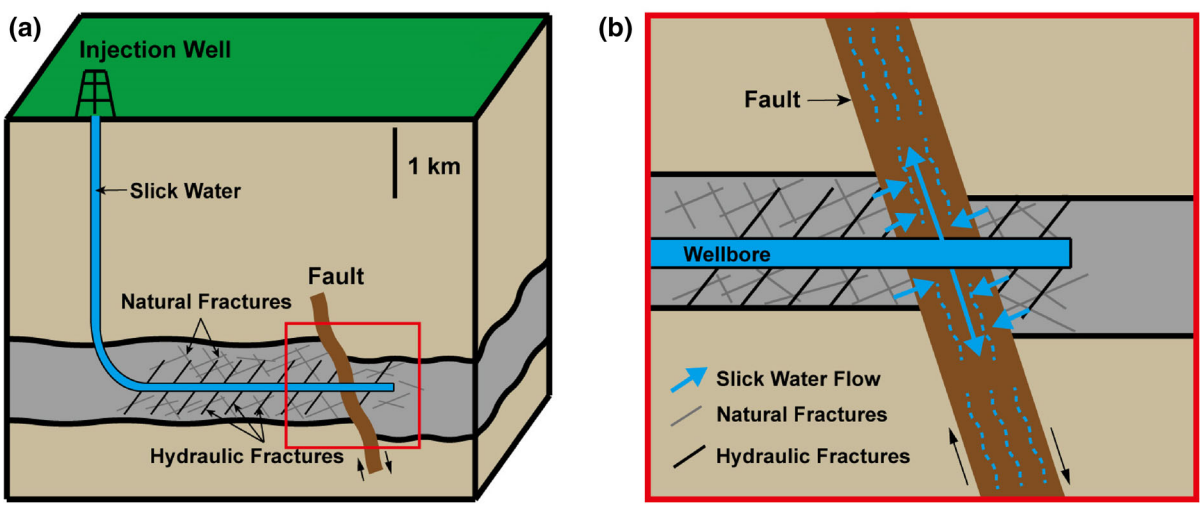

Fig. 1 **a** Schematic plot of an injection well transecting a natural fault during hydraulic fracturing. **b** The slick water can infiltrate the fault zone through several ways, like natural or hydraulic fractures and the leakage of the wellbore (Scuderi and Collettini 2018). **b** refers to the area in the red square of **a**

1998). However, the effect of the slick-water fracturing fluids on the frictional strength and stability of subsurface gouge-filled shale faults remains incompletely understood. A thorough understanding of this behavior can contribute to the confidence in designing fracture treatments in faulted reservoirs. The following examines the frictional and instability response of shale gouges permeated by slick-water fracturing fluids including the corrosive effects of friction-reducers and of clay-stabilizers. These effects are examined over an appropriate range of reservoir stresses and temperatures, including evaluation of the impact of durations of exposure. These observations are used to define the impact of slick-water fluids on gouge characteristics and transformations, and their impact on reservoir stimulation and fault stability.

2 Materials and methods

2.1 Sample preparation

A total of four samples were collected from shales of the Longmaxi Formation (Fig. 2) from Lijiawan, Niuzhai Township, Yanjin County, Zhaotong City, Yunnan Province, China (Coordinates: N 28° 07′ 55″, E 104° 26′ 40″). Lijiawan is located in the Zhaotong national shale gas demonstration area (Liang et al. 2016) on the southern edge of the Sichuan Basin, China. The Sichuan Basin is currently the major region for shale gas extraction and production in China (Yang et al. 2014). Outcrops of Upper Ordovician Wufeng Formation shale and Lower Silurian Longmaxi Formation shale are widely distributed around Lijiawan and both shales are important target zones for shale gas exploration and recovery in China (Borjigin et al. 2017; Luo et al. 2016).

Unweathered fresh samples of the Longmaxi formation shales were recovered then cleaned for surface impurities. The samples were crushed and sieved to < 75 μm size fraction to simulate gouge. The particle size distribution of the gouge samples was measured by laser classifier (instrument type: Mastersizer 2000). The median particle sizes (D50) of resulting shale gouges 1#, 2#, 3# and 4# were 2.0, 4.9, 3.8, and 2.8 μm (Fig. 3), respectively. X-ray diffraction (XRD) data were recovered using a Rigaku D/max-rB X-ray diffractometer at the Micro Structure Analytical Laboratory at Peking University, Beijing, China. All diffraction data were recorded from a starting angle of 3° to a completion angle of 70°. All four fabricated shale gouges (Fig. 4 and Table 1) contained quartz, feldspars and clay minerals. Shale 1# consisted mainly of tectosilicate minerals, without carbonates; shale 2# contained a small amount of carbonates with relative proportions as carbonates < phyllosilicates < tectosilicates; shale 3# with moderate amounts of carbonates contained similar proportions of tectosilicates, phyllosilicates and carbonates; and shale 4# was dominated by carbonates.

2.2 Slick-water

The slick-water used in this study consisted of 0.1 vol% drag reduction agent (friction reducer) and 4.0 wt% clay control agents (Aderibigbe and Lane 2013; Al-Muntasheri 2014). Other additives, including cleanup agents and de-emulsifiers, are ignored and excluded. The drag reduction agent is the water-soluble emulsion, polyacrylamide, manufactured by the SNF Group. The clay control agent is a mixture of potassium chloride (KCl) and ammonium chloride (NH_4Cl). The resulting "slick-water" is weakly acidic with an initial pH of 5.8. The shale gouges were treated with the slick-water prior to conducting the friction experiments. Each 15 g sample of shale gouge was saturated with 500 mL of slick-water for 5-days at room temperature. For comparison, a double dose of 1000 mL slick-water was also used for the same 15 g gouge samples of shale 4#, also for a 5-day treatment. The pH value of the slick water was monitored during the treatment with the results shown in Fig. 5. For the slick-water applied to shale gouges 2#, 3#, and 4#, the pH value increased from 5.8 to 7.0 within 1 day. In contrast, the pH of the slick-water applied to shale gouge 1# remained unchanged. The neutralization of the water applied to shale gouges 2#, 3#, and 4# results from the dissolution of carbonates within the shale. The remaining slick-water was removed after the 5-day treatment and the gouges dried at room temperature for further XRD analysis and friction experiments. The XRD results (Table 2) indicate the dissolution of 4–7 wt% calcite and dolomite in shale gouges 2#, 3#, and 4# but with the formation of 2–3 wt% magnesite and < 1 wt% kaolinite.

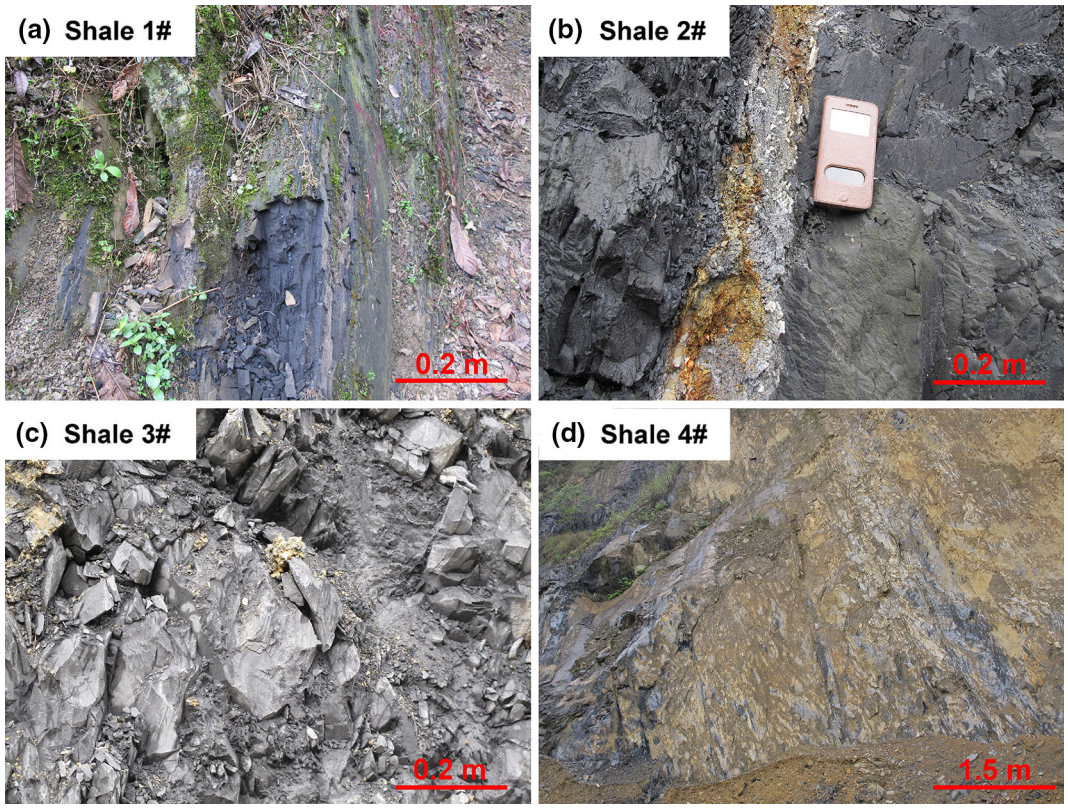

Fig. 2 Outcrop of the four Longmaxi Formation shales, **a** shale 1#, **b** shale 2#, **c** shale 3#, and **d** shale 4#

2.3 Testing apparatus and procedure

The friction experiments were carried out using a high-pressure and high-temperature argon-gas confined triaxial shear apparatus (Fig. 6) at the Institute of Geology, China Earthquake Administration (He et al. 2016; Zhang et al. 2017b). A 1-mm-thick sample of shale gouge was sandwiched between two stainless-steel cylindrical blocks transected at 35° inclination to the axis. The length and diameter of the driving steel blocks were 40 and 19.8 mm, respectively. The saw cut surfaces were carved with 1-mm-width and 0.2-mm-height grooves to avoid shear along this gouge-platen interface (Moore and Lockner 2011). The upper driving block was drilled with two thoroughgoing 2.5-mm-diameter boreholes to maintain the effective contact of pore fluid with the shale gouges. Brass filters were inserted into the ends of the two boreholes to prevent extrusion of the gouge. After the gouge was placed between the two steel driving blocks, the gouge-filled cylinder was inserted into a thin copper jacket with high-hardness tungsten carbide and corundum on both sides. The space between the thin copper jacket and furnace was filled with high thermal- but low electrical-conductivity boron nitride. O-rings on both sides of the copper jacket excluded the incursion of pressurized argon gas into the shale gouge.

During the experiment, a confining pressure of 60 MPa, a pore fluid pressure of 30 MPa and a temperature of 90 °C were applied to approximate the in situ conditions of an injection well at a depth of 2.3 km (Chen et al. 2017). When the fault assembly was placed in the pressure vessel, the confining pressure and pore fluid pressure were increased to approximately two thirds of the targeted values, since the pressure the argon confining fluid increases with an increase in temperature. Both deionized (DI) water and the slick-water mixture were separately adopted as pore fluids representing either untreated or treated shale gouges, respectively. Then the furnace was heated to the desired value, followed by adjusting the confining pressure and pore fluid pressure to the targeted values. The temperature was independently

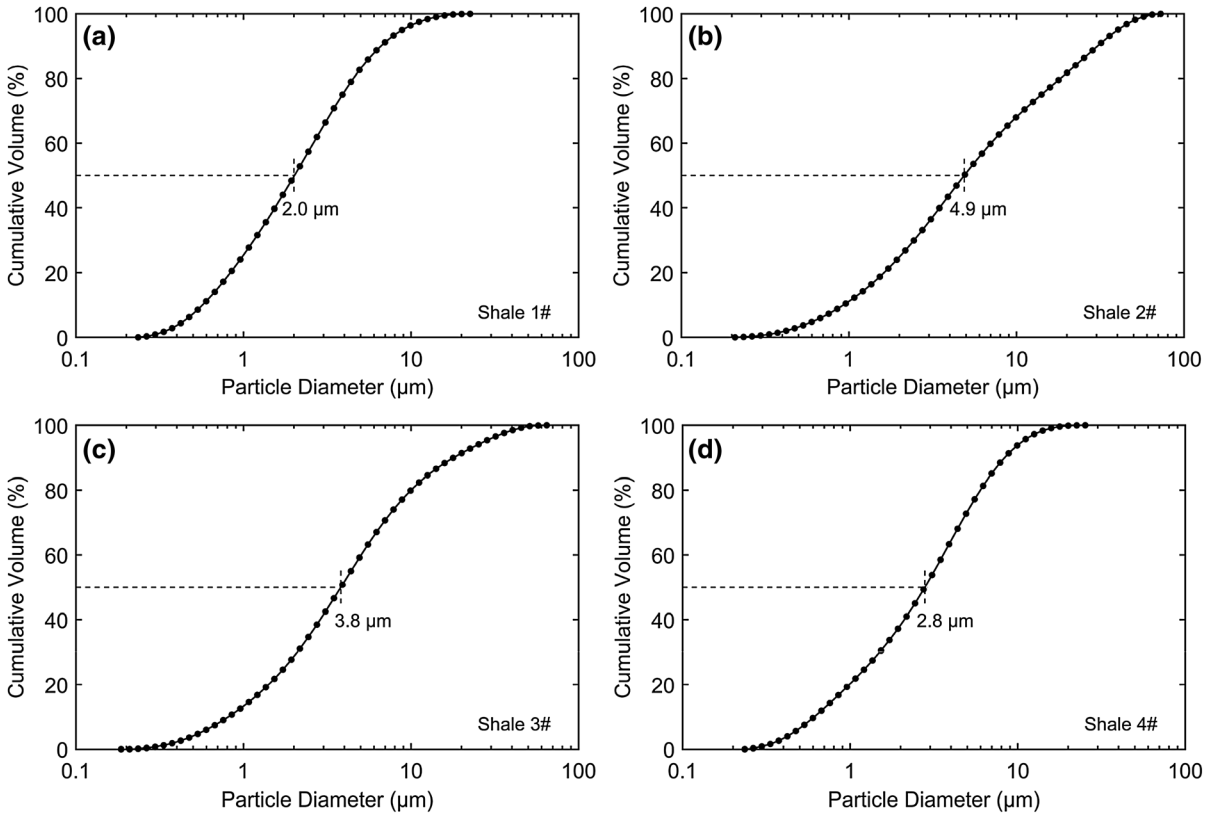

Fig. 3 Particle size distribution of the four shale gouges, **a** shale 1#, **b** shale 2#, **c** shale 3#, and **d** shale 4#

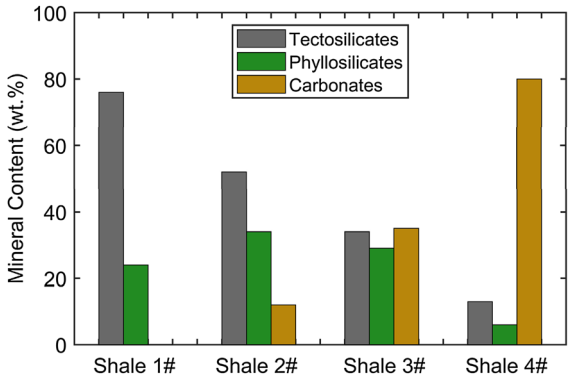

Fig. 4 Mineral compositions of the four shale gouges. Tectosilicate minerals include quartz, albite, and microcline; phyllosilicate minerals include smectite, illite, kaolinite, and chlorite; carbonate minerals include calcite, dolomite, and magnesite

Table 1 Mineral compositions (wt%) of the four shale gouges

Gouges	Qtz	Alb	Mic	Cal	Dol	Pyr	Ill	Chl	I/S
1#	68	5	3	–	–	–	22	–	2
2#	34	13	5	9	3	2	22	7	5
3#	25	6	3	30	5	2	17	7	5
4#	4	6	3	80	–	1	4	1	1

Qtz, quartz; Alb, albite; Mic, microcline; Cal, calcite; Dol, dolomite; Pyr, pyrite; Ill, illite; Chl, chlorite; I/S, illite/smectite mixed layer

monitored by thermocouple during the experiments (Fig. 6).

At the initiation of the experiment, the gouge was sheared at a constant axial displacement rate of 1 μm/s. Once steady state friction was achieved, the axial loading rate was stepped between 1 and 0.1 μm/s, corresponding to shear velocities of 1.22 and 0.122 μm/s along the shearing direction of the gouge, to acquire the velocity dependence of gouge friction. All experimental data were recorded at a sampling frequency of 10 Hz for the experiment matrix shown in Table 3.

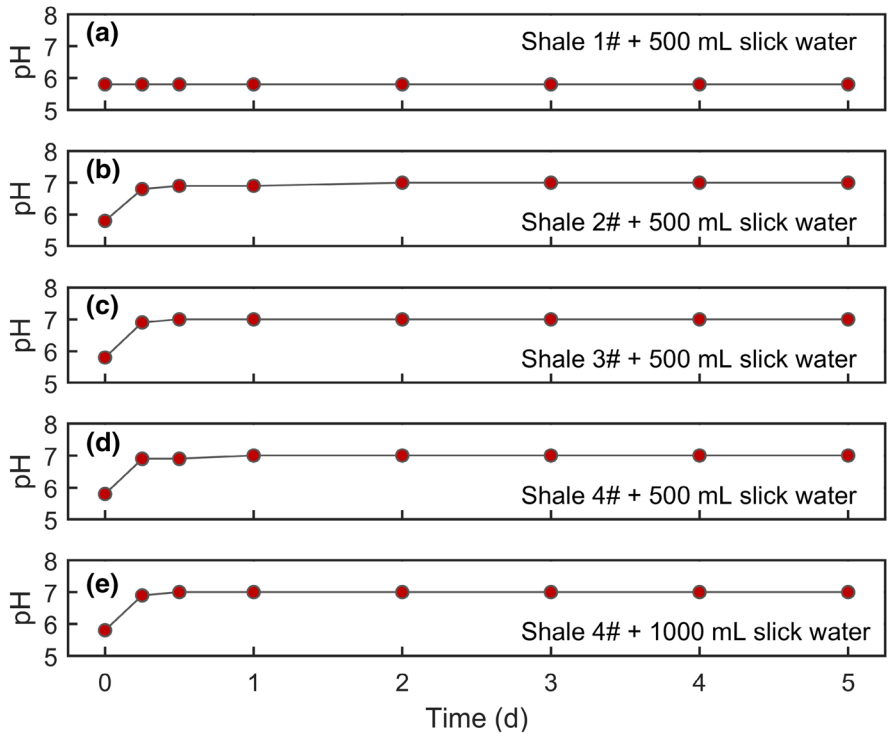

Fig. 5 pH value versus saturation time for the four shale gouges during the 5-day exposure to slick-water treatment

Table 2 Mineral compositions (wt%) of the shale gouges following slick water treatment

Gouges	Qtz	Alb	Mic	Cal	Dol	Mag	Pyr	Ill	Chl	I/S	Kao
2#-500SW	33	11	7	6	2	3	2	23	7	6	–
3#-500SW	23	7	3	27	4	3	2	19	7	5	–
4#-500SW	3	6	2	75	–	< 2	1	6	2	3	< 1
4#-1000SW	3	7	3	73	–	< 2	1	6	2	3	< 1

500 SW means that the 15 *g* shale gouge sample was treated with 500 mL of slick-water

Mag magesite, *Kao* kaolinite

2.4 Data analysis

All recorded experimental data were corrected following the method described by He et al. (2006) to compensate for the variation in shear area with offset and for the shear resistance of the copper jacket (Moore and Lockner 2008). The coefficient of friction μ reflects the magnitude of gouge frictional strength, calculated as,

$$\mu = \tau/(\sigma_n - P_f) \tag{1}$$

where τ, σ_n and P_f represent the applied shear stress, normal stress and pore fluid pressure, respectively. A laboratory derived rate- and state- friction (RSF) constitutive law was employed to evaluate the velocity dependence of gouge friction (Dieterich 1978, 1979; Marone 1998; Ruina 1983), expressed as,

$$\mu = \mu_0 + a\ln\left(\frac{V}{V_0}\right) + b\ln\left(\frac{V_0\theta}{D_c}\right) \tag{2}$$

$$\frac{d\theta}{dt} = 1 - \frac{V\theta}{D_c}\,(\text{Dieterich law}) \tag{3}$$

where μ_0 is the reference steady state coefficient of friction at the reference shear velocity V_0, μ is the instantaneous coefficient of friction at the shear

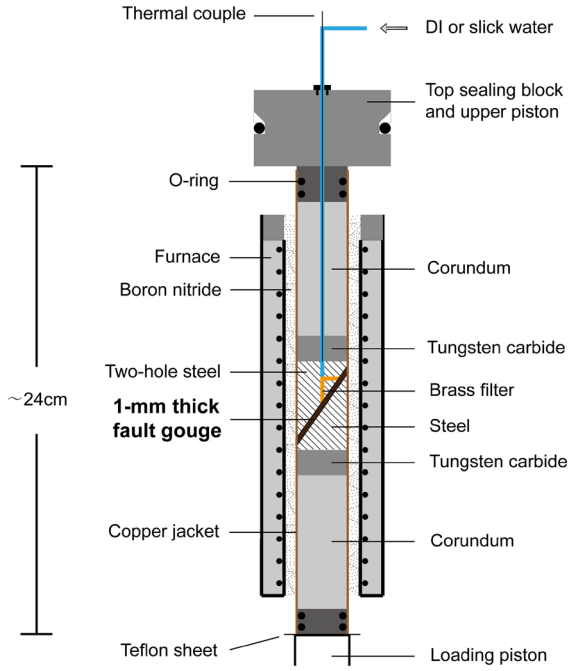

Fig. 6 Schematic of the triaxial shear assembly used for the friction experiments. The temperature was measured at the midpoint of the gouge sample

velocity V, a and b are two constants and reflect the direct and evolutional effects from the velocity change, respectively, θ is a state variable, D_c is the critical slip distance required to transit from the past state to a new steady state, and t is time (Fig. 7). At steady state friction, θ remains constant with the variation of time and thus $d\theta/dt = 0$. Then, the friction stability parameter $(a - b)$ can be obtained from Eqs. (2) and (3), as,

$$a - b = \frac{\Delta\mu_{ss}}{\Delta \ln(V)} \tag{4}$$

where $\Delta\mu_{ss}$ denotes the difference between the steady state coefficients of friction before then after the velocity step. Positive $(a - b)$ indicates that the coefficient of friction increases with an increase in shear velocity and the gouge exhibits velocity strengthening behavior, promoting inherently stable sliding (Fig. 7). To the contrary, gouges exhibiting negative $(a - b)$ are velocity weakening and may potentially promote unstable sliding (Marone 1998). The slope was detrended in calculating values of $(a - b)$, as shown in Fig. 7b.

3 Results

The coefficient of friction versus shear displacement curves for the four untreated and slick-water treated shale gouges are shown in Figs. 8 and 9. Each experiment exhibits a near linear increase in friction until achieving a steady state. The decrease in frictional strength μ of shale gouges 2#, 3#, 4#, 2#-500SW, 3#-500SW, 4#-500 SW, and 4#-1000SW (Figs. 8 and 9) may be attributed to the alignment of clay minerals (Saffer et al. 2001) during shearing. We evaluate the steady state coefficient of friction at ~ 2.75 mm shear displacement and a shear velocity of 1.22 μm/s for all experiments with the results presented in Fig. 10 and Table 4. The frictional strengths of shale gouges 2#, 3#, and 4# (μ = 0.50–0.64) are broadly consistent with gouges in previous studies showing similar contents of phyllosilicates (20–35 wt%) (Kohli and Zoback 2013; Zhang et al. 2019). Shale gouge 2# exhibits the lowest frictional strength ($\mu \approx 0.5$) among the four shale gouges due to its highest phyllosilicate content (34 wt%). Consistent

Table 3 Experiment matrix. 500SW indicates that the gouge was treated by 500 mL of slick water

Shale gouges	σ_c (MPa)	P_f (MPa)	T (°C)	Pore fluids	Velocity steps (μm/s)	l_{final} (mm)
1#	60	30	90	DI water	1.22–0.122–1.22	3.21
2#	60	30	90	DI water	1.22–0.122–1.22	3.21
3#	60	30	90	DI water	1.22–0.122–1.22	3.24
4#	60	30	90	DI water	1.22–0.122–1.22	3.49
1#-500SW	60	30	90	Slick water	1.22–0.122–1.22	3.50
2#-500SW	60	30	90	Slick water	1.22–0.122–1.22	3.31
3#-500SW	60	30	90	Slick water	1.22–0.122–1.22	3.45
4#-500SW	60	30	90	Slick water	1.22–0.122–1.22	3.59
4#-1000SW	60	30	90	Slick water	1.22–0.122–1.22	3.56

σ_c confining pressure, P_f pore fluid pressure, T temperature, l_{final} final shear displacement

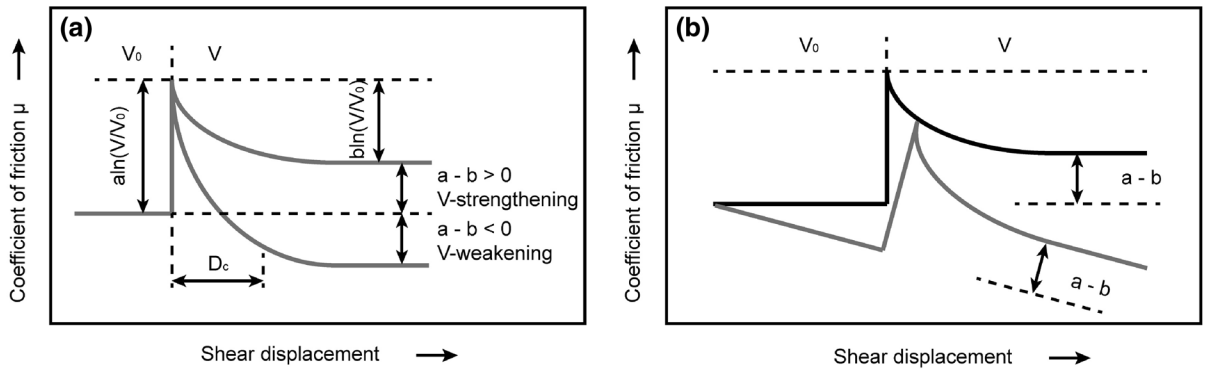

Fig. 7 **a** Rate and state friction (RSF) model ($V > V_0$) showing the two responses of velocity strengthening ($a - b > 0$) and velocity weakening ($a - b < 0$) behavior. **b** Schematic plot showing the slope was detrended in the calculation of ($a - b$)

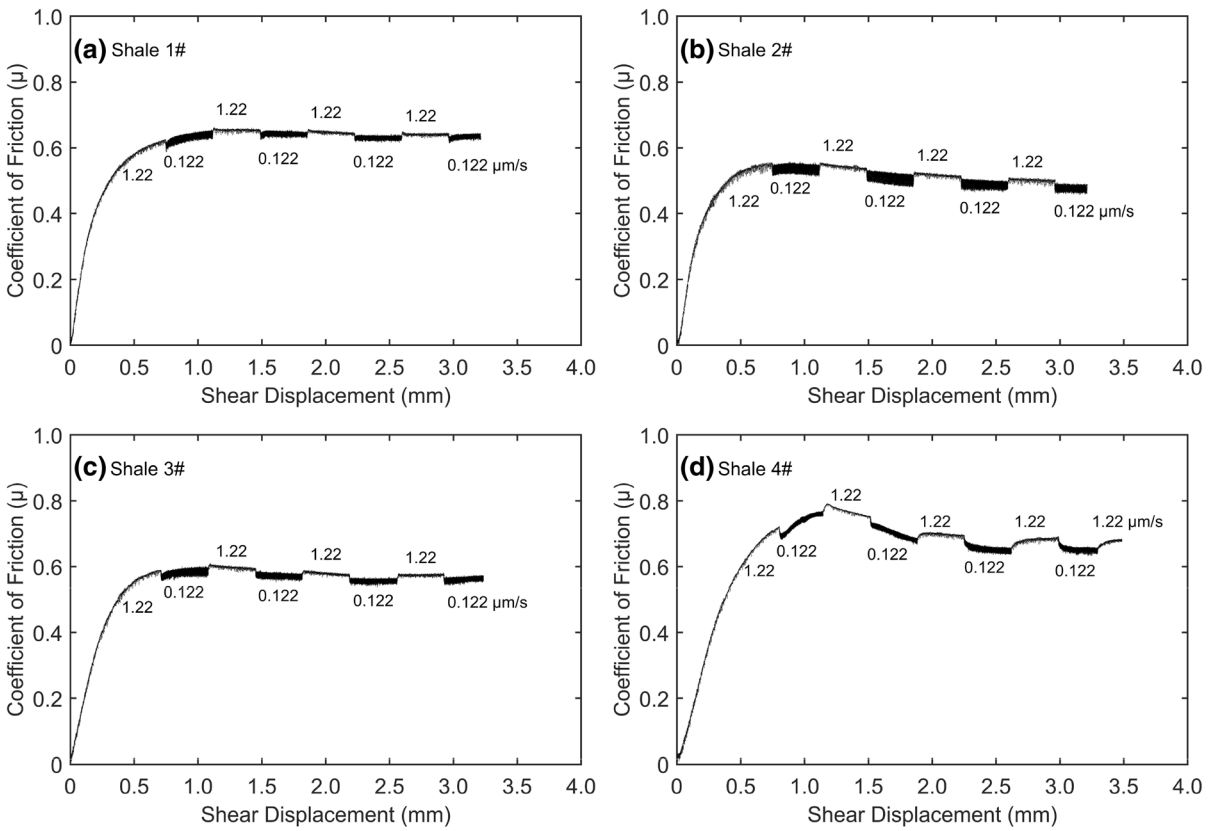

Fig. 8 Friction-vs-shear displacement curves for the four untreated shale gouges, **a** shale 1#, **b** shale 2#, **c** shale 3#, and **d** shale 4#

with this, shale gouge 4#, with the lowest phyllosilicate content (6 wt%), shows the highest frictional strength ($\mu \approx 0.68$). Many previous studies on friction of natural or synthetic gouges indicate that phyllosilicate-rich gouges show much lower frictional strength than phyllosilicate-poor gouges (Giorgetti et al. 2015; Ikari et al. 2011; Moore and Lockner 2011; Numelin et al. 2007). The frictional strength of shale gouge 1# ($\mu \approx 0.64$) is higher than that of shale gouges 2# and 3# due to its higher tectosilicate content (76 wt%), but still lower than that of shale gouge 4# due to its higher phyllosilicate content (24 wt%). The

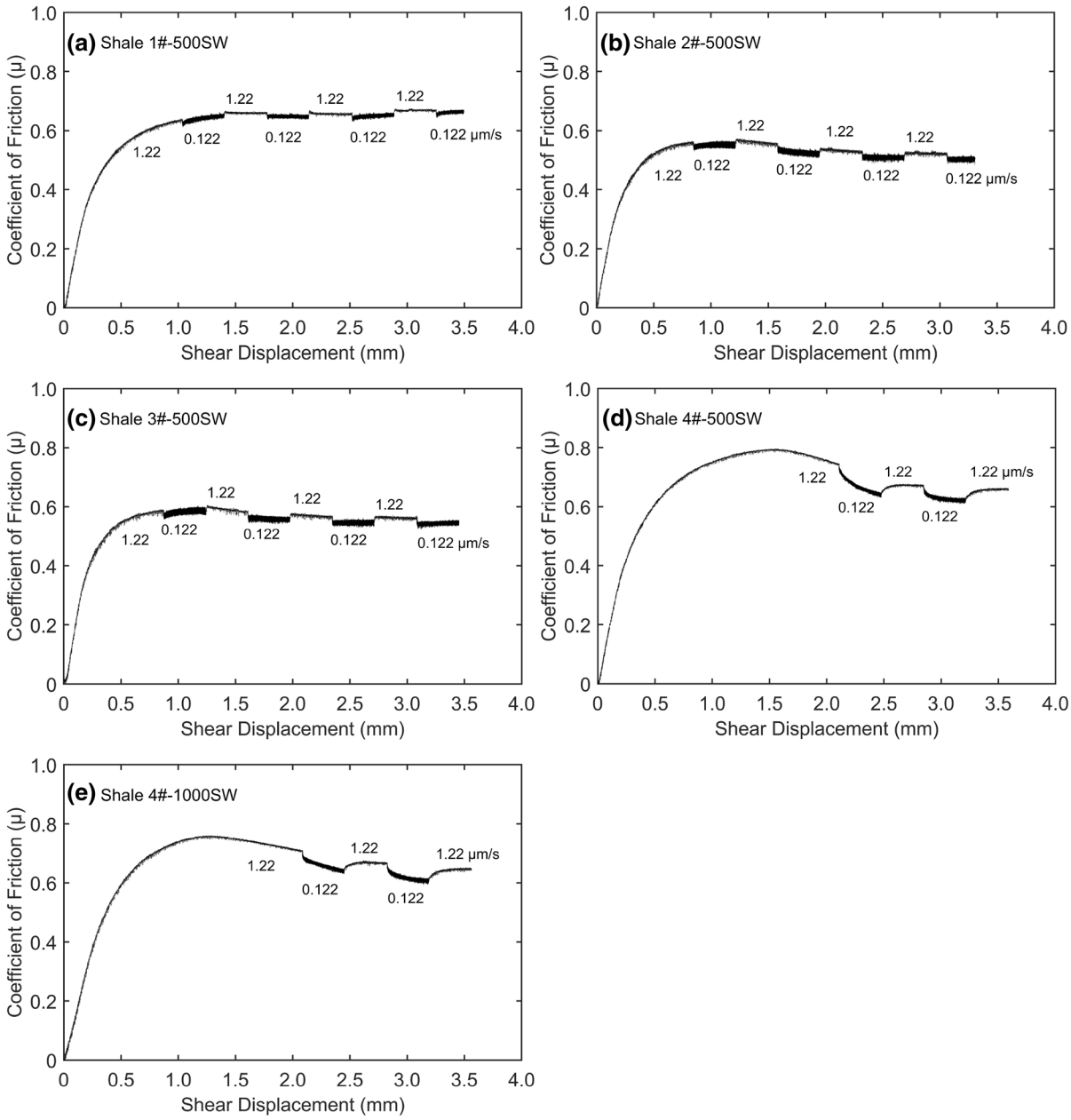

Fig. 9 Friction-vs-shear displacement curves for the four 500/1000 mL slick-water treated shale gouges, **a** shale 1#-500SW, **b** shale 2#-500SW, **c** shale 3#-500SW, **d** shale 4#-500SW, and **e** shale 4#-1000SW

difference in frictional strengths for the four untreated and slick-water treated shale gouges is within 0.02 (Table 4 and Fig. 10), implying that the slick water exerts little influence on the frictional strength of the studied shale gouges.

Values of velocity dependence $(a - b)$ were calculated following the method described in Sect. 2.4 with the results presented in Fig. 11 and Table 4. All shale gouges exhibit positive values of $(a - b)$, indicating that these shale gouges would promote stable sliding. Values of $(a - b)$ are similar for both

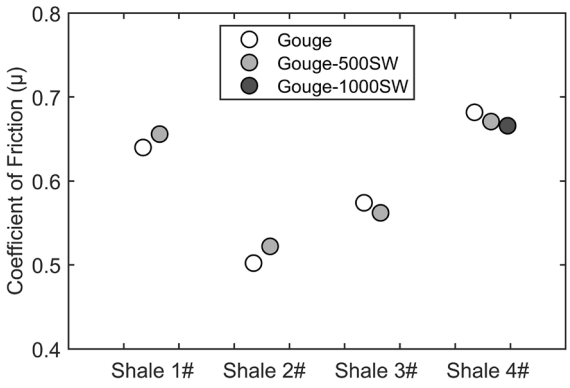

Fig. 10 Comparison of coefficient of friction μ for the four untreated and 500/1000 mL slick-water treated shale gouges

untreated and slick-water treated shale gouges 1#, 2#, and 3# (Fig. 11a). In contrast, a slight increase in values of $(a - b)$ is observed for shale gouge 4# with an increase in the volume of slick-water applied to the sample (Fig. 11b), and possibly resulting from an increase in relative phyllosilicate content during slick-water treatment (Table 2) (as carbonate is dissolved then removed). As apparent in previous observations, an increase in phyllosilicate content in gouges increases the frictional stability (increasing positive $(a - b)$) and thus promotes stable sliding (Takahashi et al. 2007; Tembe et al. 2010; Wang et al. 2017).

4 Discussion

4.1 Effect of acidic slick-water on gouge friction

From the XRD results (Tables 1 and 2) and from the observed variation in pH (Fig. 5), the acidic slick-water treatment may trigger a series of chemical reactions in the gouge. These candidate reactions are defined below and represent dissolution of calcium (Eqs. (5) and (6)) into an aqueous component and transformations to either magnesite (Eq. (7)) or kaolinite (Eqs. (8) and (9)).

$$\mathrm{CaCO_3(calcite)} + 2\mathrm{H^+} \rightarrow \mathrm{Ca^{2+}} + \mathrm{CO_2} + \mathrm{H_2O} \quad (5)$$

$$\mathrm{CaMg(CO_3)_2(dolomite)} + 4\mathrm{H^+} \rightarrow \mathrm{Ca^{2+}} + \mathrm{Mg^{2+}} + 2\mathrm{H_2O} + 2\mathrm{CO_2} \quad (6)$$

$$\mathrm{CaCO_3(calcite)} + \mathrm{Mg^{2+}} \rightarrow \mathrm{MgCO_3(magnesite)} + \mathrm{Ca^{2+}} \quad (7)$$

Table 4 Magnitudes of coefficient of friction μ and its velocity dependence $(a - b)$ for all friction experiments

Shale gouges	Coefficient of friction μ	Velocity step (μm/s)	Values of $(a - b)$
1#	0.640	0.122–1.22	0.0049 ± 0.0005
		1.22–0.122	0.0047 ± 0.0004
2#	0.502	0.122–1.22	0.0083 ± 0.0009
		1.22–0.122	0.0093 ± 0.0004
3#	0.574	0.122–1.22	0.0068 ± 0.0006
		1.22–0.122	0.0079 ± 0.0001
4#	0.682	0.122–1.22	0.0147 ± 0.0010
		1.22–0.122	0.0159 ± 0.0007
1#-500SW	0.656	0.122–1.22	0.0051 ± 0.0012
		1.22–0.122	0.0047
2#-500SW	0.522	0.122–1.22	0.0068 ± 0.0006
		1.22–0.122	0.0084 ± 0.0003
3#-500SW	0.562	0.122–1.22	0.0073 ± 0.0008
		1.22–0.122	0.0089 ± 0.0005
4#-500SW	0.671	0.122–1.22	0.0166
		1.22–0.122	0.0183
4#-1000SW	0.666	0.122–1.22	0.0176
		1.22–0.122	0.0207

Magnitudes of $(a - b)$ for shale gouges 1#, 2#, 3#, 1#-500SW, 2#-500SW, and 3#-500SW were calculated from the second velocity step to ensure that all velocity steps were in their steady states. For shale gouges 4#, 4#-500SW, and 4#-1000SW, only the final velocity steps at steady state were adopted to calculate the values of $(a - b)$

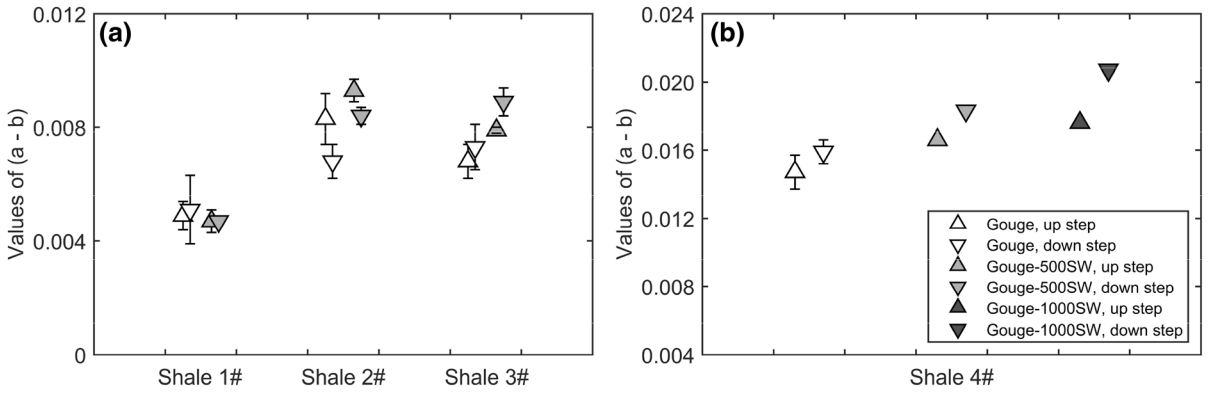

Fig. 11 Comparison of velocity dependence of friction $(a - b)$ for the four untreated and 500/1000 mL slick-water treated shale gouges, **a** untreated and slick-water treated shale gouges 1#, 2#, and 3#, and **b** untreated and slick-water treated shale gouges 4#

$$2NaAlSi_3O_8(\text{albite}) + 2CO_2 + 11H_2O \rightarrow Al_2Si_2O_5(OH)_4(\text{kaolinite}) + 2Na^+ + 2HCO_3^- + 4H_4SiO_4 \quad (8)$$

$$2KAlSi_3O_8(\text{microcline}) + 2CO_2 + 11H_2O \rightarrow Al_2Si_2O_5(OH)_4(\text{kaolinite}) + 2K^+ + 2HCO_3^- + 4H_4SiO_4 \quad (9)$$

Firstly, the calcite and dolomite may be dissolved during acidic slick-water treatment according to the reactions of Eqs. (5) and (6), and consistent with the results of previous experiments (Dieterich et al. 2016; Sun et al. 2018). Secondly, the precipitation of a small amount of magnesite indicates that a replacement reaction may occur between calcium and magnesium ions, as noted in the reaction of Eq. (7) (Zilberbrand 1999). The magnesium ions may source, not only from the reaction between dolomite and the hydrogen ions (Eq. (6)), but also from the dissolution of illite and smectite in the slick water (Ali and Hascakir 2017). Thirdly, the occurrence of kaolinite may also result from the reaction of albite or microcline with carbon dioxide (CO_2) and water (H_2O) through the reactions of Eqs. (8) and (9) (Nightingale et al. 2009; Zhou et al. 2012). During the friction experiments, high temperatures (T = 90 °C) would further accelerate the reaction rates between the slick-water (pore fluids) and the treated shale gouges. However, due to the merely weakly-acidic slick-water and the limited resulting mineral alteration, the slick-water treatment is shown to have negligible effect on the frictional strength and stability at short timescales for the shale gouges studied here, except for on the frictional stability of shale gouge 4#.

Since the slick-water u–sed in our experiments is only weakly-acidic (pH = 5.8) and applied for only a very short reaction time prior to the friction experiments, there is limited potential for the dissolution of carbonate minerals (Table 2). However, a significant amount of carbonate might be dissolved during acid fracturing over extended durations (Nieto et al. 2008; Wu and Sharma 2017). Reservoir shales can be indexed relative to the proportions of three key groups of minerals i.e., tectosilicates, phyllosilicates and carbonates (Fang et al. 2017; Kohli and Zoback 2013), ignoring the content of trace components, such as pyrite. The dissolution of carbonate increases the relative contents of tectosilicates and phyllosilicates, since tectosilicates (wt%) + phyllosilicates (wt%) + carbonates (wt%) = 1. This mineral alteration can exert a control on the frictional strength and stability of gouge-filled faults.

Previous laboratory results demonstrate that, for this ternary grouping of minerals (tectosilicates-phyllosilicates-carbonates), tectosilicate-rich or carbonate-rich gouges are prone to exhibit higher frictional strength but unstable response, while phyllosilicate-rich gouges show the opposite trend (Fang et al. 2018; Ikari et al. 2011) of low-friction and high-stability. For binary groupings of minerals (tectosilicates-phyllosilicates or carbonates-phyllosilicates), the phyllosilicate content controls the fault frictional response.

Meanwhile, > 20–30 wt% phyllosilicates can evidently lower the frictional strength and stabilize the fault (Giorgetti et al. 2015; Tembe et al. 2010; Wang et al. 2017). We consider several cases to explore the effect of carbonate dissolution on frictional properties of gouge-filled faults. First, for these binary mineral mixtures with tectosilicates-phyllosilicates, acidic slick-water will exert little influence on the frictional properties due the absence of carbonates—e.g. for shale gouge 1#. For binary mineral mixtures of carbonate-phyllosilicate, the dissolution of carbonate will increase the relative content of phyllosilicates and thus lower the frictional strength and stabilize the gouge (Giorgetti et al. 2015). Second, for ternary-mixtures with similar contents of tectosilicates, phyllosilicates, and carbonate (e.g. shale gouge 3#) or those dominated by carbonates (e.g. shale gouge 4#) or phyllosilicates, the influence of carbonate dissolution may be similar to that of carbonate-phyllosilicate gouges but also dependent on the boundary conditions such as stress, temperature and even the roughness (Fang et al. 2016; Spokas et al., 2019). For ternary-mixtures dominated by tectosilicates (e.g. shale gouge 2#), the dissolution of carbonates may promote either fault stability or instability with the gouge frictional properties depending on the relative contents of tectosilicates and phyllosilicates.

Though the dissolution of carbonate minerals may typically stabilize the gouge, it may also significantly lower the frictional strength and promote reactivation (Zhang et al. 2017a). This fault creep or aseismic slip may also induce earthquakes by modifying the local stress field and activating adjacent unstable faults during hydraulic fracturing (Eyre et al. 2019; Guglielmi et al. 2015).

4.2 Effect of clay stabilizer on gouge friction

Common clay minerals in reservoir shales include smectite, illite, chlorite and their mixed layer minerals. These clay minerals will swell in the presence of water-based fracturing fluids. Such swelling generally results in a significant increase in volume and may degrade rock strength and influence both wellbore stability and drilling efficiency (Anderson et al. 2010). To inhibit swelling during fracturing, various organic and inorganic clay stabilizers are added to fracturing fluids (Hensen and Smit 2002; Liu et al. 2004). Halide salt is one frequently adopted inorganic clay stabilizer that intercalates clay minerals and thus minimizes swelling (Anderson et al. 2010). However, from our friction measurements (Figs. 10, 11), clay swelling exerts only a minor effect on frictional properties, especially at high stresses. Several possible explanations may account for this phenomenon. At micro-scale, friction results directly from shear between mineral particles. Although clay mineral volume increases with swelling, this feature may not influence the contacts between phyllosilicates and carbonates or between phyllosilicates and tectosilicates, as depicted in Fig. 12—and therefore exert a null influence on friction. More plausibly, the applied high confining stress (σ_c = 60 MPa) may restrict significant swelling—resulting in the same null influence. Notably, our reservoir gouges are illite-dominant with significantly reduced swelling relative to smectite (Ikari et al. 2007). As a result, clay swelling will exert only minor influence on the frictional properties of shale gouges at high pressures, at least for the Longmaxi Formation shale studied here.

4.3 Implications for shale reservoir stimulation

The observed dissolution of carbonate on the frictional properties of shale gouges, as a direct result of the permeation of slick-water fracturing fluids, has important implications for the stability of subsurface gouge-filled faults and the resulting seismic potential of shale reservoirs. The infiltration of acidic slick-water into faults not only elevates pore fluid pressures, but may also transform the mineralogic composition, and thereby affect the frictional strength and stability of faults. As carbonate-rich shales are common, including in the Bakken, Eagle Ford (Wu and Sharma 2017) and Longmaxi shales (this study), the frictional stability data of shale 4# suggest that fault stability can indeed be impacted by slick-water treatment.

Our results also suggest possible mechanisms for delayed earthquakes following hydraulic fracturing. Previous studies indicate that some induced earthquakes are delayed for several months or years (van der Elst et al. 2013; Yeck et al. 2016) following injection. One possible explanation for delayed earthquakes is due to delayed poromechanical changes in

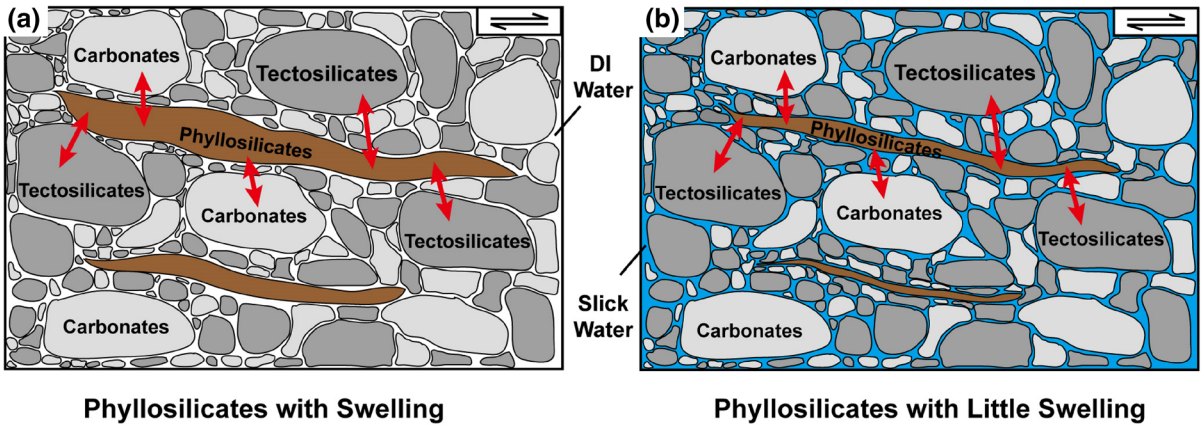

Fig. 12 Schematics showing **a** the swelling of phyllosilicates in DI water, and **b** the minor influence of swelling of phyllosilicates in slick-water

effective stresses (Eyre et al. 2019; Segall and Lu 2015) that change the stress regime. A complementary mechanism is one that relies on a reduction in strength resulting from mineralogical transformations explored in this study. The interplay between the slick-water fracturing fluid and fault gouge material may affect the timing of subsurface fault nucleation and further promote earthquakes (Westaway and Burnside 2019).

5 Conclusions

We report triaxial shear experiments on simulated shale gouges at $\sigma_c = 60$ MPa, $P_f = 30$ MPa, $T = 90$ °C and shear velocities of 0.122–1.22 μm/s, to define the effect of slick-water infiltration on gouge frictional strength and stability. For shale gouges not exposed to slick-water treatment, the phyllosilicate-rich shale gouges show a lower frictional strength than the carbonate-rich shale gouge. All shale gouges exhibit strong velocity strengthening, indicative of promoting stable fault sliding. Comparison between the frictional response of the untreated and slick-water-treated shale gouges implicate a series of chemical transformations driven by the acidic slick-water that are capable of reducing carbonate content by both dissolution and transformation. The dissolution of relatively minor amounts of carbonate are shown to exert scant influence on frictional strength but enhance the fault stability as a result of the relative increase in phyllosilicate content. Clay swelling can be inhibited by the use of clay stabilizers but these have little influence on fault strength and stability, especially at high pressures—although this requires further confirmation for other combinations of stabilizers and reservoir rocks. These experiments suggest mechanisms responsible for slick-water corrosion in shale fault gouges with broad implications for the potential for triggering earthquakes both during and after the stimulation of shale gas reservoirs.

Acknowledgements This work is supported by International Exchange Program for Graduate Students, Tongji University (No. 201902014), the Key Innovation Team Program of Innovation Talents Promotion Plan by MOST of China (No. 2016RA4059), and National Natural Science Foundation of China (No. 41772286). We thank Changrong He, Jianye Chen, Wenming Yao and Yang Liu for laboratory assistance. Raw data of all friction experiments are available at the pictures and tables.

Compliance with ethical standards

Conflict of interest The authors declare that they have no conflict of interest.

References

Aderibigbe AA, Lane RH (2013) Rock/fluid chemistry impacts on shale fracture behavior. In: SPE international symposium on oilfield chemistry, 8–10 April, The Woodlands, Texas, USA. https://doi.org/10.2118/164102-ms

Ali M, Hascakir B (2017) Water/rock interaction for Eagle Ford, Marcellus, Green river, and Barnett shale samples and implications for hydraulic-fracturing-fluid engineering. SPE J 22(1):162–171. https://doi.org/10.2118/177304-PA

Al-Muntasheri GA (2014) A critical review of hydraulic-fracturing fluids for moderate- to ultralow- permeability

formations over the last decade. SPE Prod Oper 29(4):243–260. https://doi.org/10.2118/169552-PA

Anderson RL, Ratcliffe I, Greenwell HC, Williams PA, Cliffe S, Coveney PV (2010) Clay swelling—a challenge in the oilfield. Earth Sci Rev 98(3–4):201–216. https://doi.org/10.1016/j.earscirev.2009.11.003

Arthur JD, Hochheiser HW, Coughlin BJ (2011) State and federal regulation of hydraulic fracturing: a comparative analysis. In: SPE hydraulic fracturing technology conference, 24–26 January, The Woodlands, Texas, USA. https://doi.org/10.2118/140482-ms

Borjigin T, Shen B, Yu L, Yang Y, Zhang W, Tao C, Xi B, Zhang Q, Bao F, Qin J (2017) Mechanisms of shale gas generation and accumulation in the Ordovician Wufeng-Longmaxi Formation, Sichuan Basin, SW China. Pet Explor Dev 44(1):69–78. https://doi.org/10.1016/S1876-3804(17)30009-5

Chen Z, Shi L, Xiang D (2017) Mechanism of casing deformation in the Changning–Weiyuan national shale gas demonstration area and countermeasures. Nat Gas Ind B 4(1):1–6. https://doi.org/10.1016/j.ngib.2017.07.001

Clark JB (1949) A hydraulic process for increasing the productivity of wells. J Pet Technol 1(01):1–8. https://doi.org/10.2118/949001-g

Davies R, Foulger G, Bindley A, Styles P (2013) Induced seismicity and hydraulic fracturing for the recovery of hydrocarbons. Mar Pet Geol 45:171–185. https://doi.org/10.1016/j.marpetgeo.2013.03.016

Diao Y, Espinosa-Marzal RM (2018) The role of water in fault lubrication. Nat Commun. https://doi.org/10.1038/s41467-018-04782-9

Dieterich JH (1978) Time-dependent friction and the mechanics of stick-slip. Pure Appl Geophys 116(4–5):790–806. https://doi.org/10.1007/BF00876539

Dieterich JH (1979) Modeling of rock friction: 1. Experimental results and constitutive equations. J Geophys Res. https://doi.org/10.1029/JB084iB05p02161

Dieterich M, Kutchko B, Goodman A (2016) Characterization of Marcellus Shale and Huntersville Chert before and after exposure to hydraulic fracturing fluid via feature relocation using field-emission scanning electron microscopy. Fuel 182:227–235. https://doi.org/10.1016/j.fuel.2016.05.061

Eyre TS, Eaton DW, Garagash DI, Zecevic M, Venieri M, Weir R, Lawton DC (2019) The role of aseismic slip in hydraulic fracturing–induced seismicity. Sci Adv 5(8):1–11. https://doi.org/10.1126/sciadv.aav7172

Fang Y, den Hartog SA, Elsworth D, Marone C, Cladouhos T (2016) Anomalous distribution of microearthquakes in the Newberry Geothermal Reservoir: mechanisms and implications. Geothermics 63:62–73. https://doi.org/10.1016/j.geothermics.2015.04.005

Fang Y, Elsworth D, Wang C, Ishibashi T, Fitts JP (2017) Frictional stability-permeability relationships for fractures in shales. J Geophys Res Solid Earth 122(3):1760–1776. https://doi.org/10.1002/2016JB013435

Fang Y, Elsworth D, Wang C, Jia Y (2018) Mineralogical controls on frictional strength, stability, and shear permeability evolution of fractures. J Geophys Res Solid Earth 123(5):3549–3563. https://doi.org/10.1029/2017JB015338

Giorgetti C, Carpenter BM, Collettini C (2015) Frictional behavior of talc-calcite mixtures. J Geophys Res Solid Earth 120(9):6614–6633. https://doi.org/10.1002/2015JB011970

Grossman WL (1951) Hydrafrac operations in the spraberry production, West Texas. In: Fall meeting of the petroleum branch of AIME, 3–5 October, Oklahoma City, Oklahoma. https://doi.org/10.2118/128-g

Guglielmi Y, Cappa F, Avouac JP, Henry P, Elsworth D (2015) Seismicity triggered by fluid injection–induced aseismic slip. Science 348(6240):1224–1226. https://doi.org/10.1126/science.aab0476

Guindon L (2015) Determining interwell connectivity and reservoir complexity through fracturing pressure hits and production-interference analysis. J Can Pet Technol 54(02):88–91. https://doi.org/10.2118/0315-088-JCPT

He C, Yao W, Wang Z, Zhou Y (2006) Strength and stability of frictional sliding of gabbro gouge at elevated temperatures. Tectonophysics 427(1–4):217–229. https://doi.org/10.1016/j.tecto.2006.05.023

He C, Tan W, Zhang L (2016) Comparing dry and wet friction of plagioclase: implication to the mechanism of frictional evolution effect at hydrothermal conditions. J Geophys Res Solid Earth 121(9):6365–6383. https://doi.org/10.1002/2016JB012834

Hensen EJM, Smit B (2002) Why clays swell. J Phys Chem B 106(49):12664–12667. https://doi.org/10.1021/jp0264883

Huang H, Azar JJ, Hale AH (1998) Numerical simulation and experimental studies of shale interaction with water-base drilling fluid. In: IADC/SPE Asia Pacific drilling technology, 7–9 September, Jakarta, Indonesia. https://doi.org/10.2118/47796-MS

Ikari MJ, Saffer DM, Marone C (2007) Effect of hydration state on the frictional properties of montmorillonite-based fault gouge. J Geophys Res Solid Earth 112(6):1–12. https://doi.org/10.1029/2006JB004748

Ikari MJ, Marone C, Saffer DM (2011) On the relation between fault strength and frictional stability. Geology 39(1):83–86. https://doi.org/10.1130/G31416.1

Jacoby D (2011) Global trade restrictions and related compliance issues pertaining to oil and gas production chemicals. In: Offshore technology conference, 2–5 May, Houston, Texas, USA. https://doi.org/10.4043/22005-ms

Kohli AH, Zoback MD (2013) Frictional properties of shale reservoir rocks. J Geophys Res Solid Earth 118(9):5109–5125. https://doi.org/10.1002/jgrb.50346

Liang X, Wang G, Xu Z, Zhang J, Chen Z, Xian C, Liu H, Liu C, Zhao C, Xiong S (2016) Comprehensive evaluation technology for shale gas sweet spots in the complex marine mountains, South China: a case study from Zhaotong national shale gas demonstration zone. Nat Gas Ind B 3(1):27–36. https://doi.org/10.1016/j.ngib.2016.02.003

Liu S, Mo X, Zhang C, Sun D, Mu C (2004) Swelling inhibition by polyglycols in montmorillonite dispersions. J Dispers Sci Technol 25(1):63–66. https://doi.org/10.1081/DIS-120027669

Luo Q, Zhong N, Dai N, Zhang W (2016) Graptolite-derived organic matter in the Wufeng–Longmaxi Formations (Upper Ordovician–Lower Silurian) of southeastern Chongqing, China: implications for gas shale evaluation. Int J Coal Geol 153:87–98. https://doi.org/10.1016/j.coal.2015.11.014

Marone C (1998) Laboratory-derived friction laws and their application to seismic faulting. Annu Rev Earth Planet Sci 26(1):643–696. https://doi.org/10.1146/annurev.earth.26.1.643

Moore DE, Lockner DA (2008) Talc friction in the temperature range 25°–400° C: relevance for fault-zone weakening. Tectonophysics 449(1–4):120–132. https://doi.org/10.1016/j.tecto.2007.11.039

Moore DE, Lockner DA (2011) Frictional strengths of talc-serpentine and talc-quartz mixtures. J Geophys Res Solid Earth. https://doi.org/10.1029/2010JB007881

Nieto CM, Pournik M, Hill AD (2008) The texture of acidized fracture surfaces: implications for acid fracture conductivity. SPE Prod Oper 23(3):343–352. https://doi.org/10.2118/102167-pa

Nightingale M, Johnson G, Shevalier M, Hutcheon I, Perkins E, Mayer B (2009) Impact of injected CO_2 on reservoir mine ralogy during CO_2-EOR. Energy Procedia 1(1):3399–3406. https://doi.org/10.1016/j.egypro.2009.02.129

Numelin T, Marone C, Kirby E (2007) Frictional properties of natural fault gouge from a low-angle normal fault, Panamint Valley, California. Tectonics. https://doi.org/10.1029/2005TC001916

Pagels M, Willberg DM, Edelman E, Zagorski W, Frantz J (2013) Quantifying fracturing fluid damage on reservoir rock to optimize production. In: Unconventional resources technology conference, 12–14 August, Denver, Colorado. https://doi.org/10.1190/urtec2013-180

Pedlow J, Sharma M (2014) Changes in shale fracture conductivity due to interactions with water-based fluids. In: SPE hydraulic fracturing technology conference, 4–6 February, The Woodlands, Texas, USA. https://doi.org/10.2118/168586-ms

Rubinstein JL, Mahani AB (2015) Myths and facts on wastewater injection, hydraulic fracturing, enhanced oil recovery, and induced seismicity. Seismol Res Lett 86(4):1060–1067. https://doi.org/10.1785/0220150067

Ruina A (1983) Slip instability and state variable friction laws. J Geophys Res Solid Earth 88(B12):10359–10370. https://doi.org/10.1029/JB088iB12p10359

Saffer DM, Frye KM, Marone C, Mair K (2001) Laboratory results indicating complex and potentially unstable frictional behavior of smectite clay. Geophys Res Lett 28(12):2297–2300. https://doi.org/10.1029/2001GL012869

Scuderi MM, Collettini C (2018) Fluid injection and the mechanics of frictional stability of shale-bearing faults. J Geophys Res Solid Earth 123(10):8364–8384. https://doi.org/10.1029/2018JB016084

Scuderi MM, Collettini C, Marone C (2017) Frictional stability and earthquake triggering during fluid pressure stimulation of an experimental fault. Earth Planet Sci Lett 477:84–96. https://doi.org/10.1016/j.epsl.2017.08.009

Segall P, Lu S (2015) Injection-induced seismicity: poroelastic and earthquake nucleation effects. J Geophys Res Solid Earth 120:5082–5103. https://doi.org/10.1002/2015JB012060

Spokas K, Fang Y, Fitts JP, Peters CA, Elsworth D (2019) Collapse of reacted fracture surface decreases permeability and frictional strength. J Geophys Res Solid Earth 124(12):12799–12811. https://doi.org/10.1029/2019JB017805

Sun Z, Zhang H, Wei Z, Wang Y, Wu B, Zhuo S, Zhao Z, Li J, Hao L, Yang H (2018) Effects of slick water fracturing fluid on pore structure and adsorption characteristics of shale reservoir rocks. J Nat Gas Sci Eng 51:27–36. https://doi.org/10.1016/j.jngse.2017.12.030

Takahashi M, Mizoguchi K, Kitamura K, Masuda K (2007) Effects of clay content on the frictional strength and fluid transport property of faults. J Geophys Res Solid Earth. https://doi.org/10.1029/2006JB004678

Tembe S, Lockner DA, Wong T-F (2010) Effect of clay content and mineralogy on frictional sliding behavior of simulated gouges: binary and ternary mixtures of quartz, illite, and montmorillonite. J Geophys Res Solid Earth. https://doi.org/10.1029/2009JB006383

van der Elst NJ, Savage HM, Keranen KM, Abers GA (2013) Enhanced remote earthquake triggering at fluid-injection sites in the midwestern United States. Science 341(6142):164–167. https://doi.org/10.1126/science.1238948

Vidic RD, Brantley SL, Vandenbossche JM, Yoxtheimer D, Abad JD (2013) Impact of shale gas development on regional water quality. Science. https://doi.org/10.1126/science.1235009

Wang C, Elsworth D, Fang Y (2017) Influence of weakening minerals on ensemble strength and slip stability of faults. J Geophys Res Solid Earth 122(9):7090–7110. https://doi.org/10.1002/2016JB013687

Westaway R, Burnside NM (2019) Fault "corrosion" by fluid injection: a potential cause of the November 2017 M_W 55 Korean Earthquake. Geofluids. https://doi.org/10.1155/2019/1280721

Wu W, Sharma MM (2017) Acid fracturing in shales: effect of dilute acid on properties and pore structure of shale. SPE Prod Oper 32(1):51–63. https://doi.org/10.2118/173390-pa

Yang Y, Robart CJ, Ruegamer M (2013) Analysis of US hydraulic fracturing design trends. In: SPE hydraulic fracturing technology conference, 4–6 February, The Woodlands, Texas, USA. https://doi.org/10.2118/163875-MS

Yang F, Ning Z, Liu H (2014) Fractal characteristics of shales from a shale gas reservoir in the Sichuan Basin, China. Fuel 115:378–384. https://doi.org/10.1016/j.fuel.2013.07.040

Yeck WL, Weingarten M, Benz HM, McNamara DE, Bergman EA, Herrmann RB, Rubinstein JL, Earle PS (2016) Far-field pressurization likely caused one of the largest injection induced earthquakes by reactivating a large preexisting basement fault structure. Geophys Res Lett 43(19):10198–10207. https://doi.org/10.1002/2016GL070861

Zhang F, Fang Y, Elsworth D, Wang C, Yang X (2017a) Evolution of friction and permeability in a propped fracture under shear. Geofluids. https://doi.org/10.1155/2017/2063747

Zhang L, He C, Liu Y, Lin J (2017b) Frictional properties of the South China Sea oceanic basalt and implications for strength of the Manila subduction seismogenic zone. Mar Geol 394:16–29. https://doi.org/10.1016/j.margeo.2017.05.006

Zhang F, An M, Zhang L, Fang Y, Elsworth D (2019) The role of mineral composition on the frictional and stability properties of powdered reservoir rocks. J Geophys Res Solid Earth 124(2):1480–1497. https://doi.org/10.1029/2018JB016174

Zhou X, Wang Q, Li J, Zang C, Guo Y, Zhu W (2012) Impact of late-accumulated mantle-derived CO_2 on quality of Paleogene clastic reservoir at actic area, Qin Nan Sag. Energy Explor Exploit 30(2):295–310. https://doi.org/10.1260/0144-5987.30.2.295

Zilberbrand M (1999) On equilibrium constants for aqueous geochemical reactions in water unsaturated soils and sediments. Aquat Geochem 5(2):195–206. https://doi.org/10.1023/A:1009695510370